Residual film thickness following immiscible fluid displacement in non-circular microchannels at large capillary number

Lu, Yu; Kovalchuk, Nina M.; Simmons, Mark J. H.

DOI:
10.1002/aic.16178

Residual Film Thickness following Immiscible Fluid Displacement in Noncircular Microchannels at Large Capillary Number

Yu Lu, Nina M. Kovalchuk, and Mark J. H. Simmons
School of Chemical Engineering, University of Birmingham, Birmingham B15 2TT, U.K.

DOI 10.1002/aic.16178
Published online in Wiley Online Library (wileyonlinelibrary.com)

An experimental study of the displacement of one immiscible fluid by another was performed in microchannels with circular, square and near-semicircular cross-sections, with hydraulic diameters from 100 to 200 μm. Experiments were performed over a range of capillary number, Ca, from $0.02 < Ca < 80$, with viscosity ratios between the two fluids ranging from 20 to 100. The liquid film left on the channel wall following the advance of the displacing fluid was obtained from visual measurements and a method for the estimation of mean film thickness was shown to be in good agreement with existing correlations. The addition of a surfactant (Sodium Dodecyl Sulfate, SDS) dissolved in the displacing fluid led to a reduction in the thickness of the residual film. © 2018 The Authors AIChE Journal published by Wiley Periodicals, Inc. on behalf of American Institute of Chemical Engineers *AIChE J*, 00: 000–000, 2018
Keywords: microfluidics, fluid displacement, film thickness, surfactant, capillary number

Introduction

Flows in microfluidic devices attract attention because of the benefits they offer compared to larger scale devices: very low material consumption, short residence time, and high surface area to volume ratio. The capacity of microfluidics to precisely control multiphase flows was recognized during early development in the field and is one of their important advantages. A great number of researches have been conducted using microfluidics for flow separation,[1–3] the generation of complex droplets,[4,5] chemical reaction,[6,7] and biological studies.[8]

Fluid displacement is an important topic in multiphase flow research because of applications in, for example, injection moulding, fluid transportation, and oil recovery. A primary research goal for this topic is understanding of the physics governing coating or cleaning processes within a channel, where the thickness of the liquid film left on the wall following the passage of the displacing fluid is a critical factor. Fairbrother and Stubbs[9] examined the liquid layer surrounding a long bubble passing through water and suggested the thickness of the liquid film left on wall was dependent on the capillary number $Ca = \mu u/\sigma$, where μ is the liquid dynamic viscosity, u is the bubble velocity, and σ is the surface or interfacial tension. They also proposed that the film thickness could be independent of the bubble length, for lengths greater than 1.5 times of the channel inner diameter.

Correspondence concerning this article should be addressed to Yu Lu at y.lu.3@pgr.bham.ac.uk.

Taylor[10] extended this work using 2 mm and 3 mm circular tubes with Ca values up to 1.9 and proposed an asymptotic value of the fraction of liquid left on wall to be ~0.55. In the same year, Bretherton[11] developed a model for $Ca < 0.01$. Irandoust and Andersson[12] studied the film thickness of rising Taylor bubble in channels of 1–2 mm diameter. Their correlation was verified by experimental results for $Ca < 2.0$. Similarly to Fairbrother and Stubbs,[9] they found the film thickness to be independent of bubble length for lengths greater than the channel diameter; this result was also observed by Ratulowski and Chang[13] who studied the transport of bubbles in capillaries.

Aussillous and Quere[14] developed a phenomenological model which provided a good fit to to the experimental data of Taylor,[11] known as Taylor's law. They also examined the effect of channel sizes on the film thickness and found that a larger channel diameter resulted in larger film thickness. Han and Shikazono[15] measured the film thickness in circular microchannels using a novel laser focus displacement method and developed an empirical model that was able to predict the film thickness depending on the values of Ca, Reynolds number ($Re = \rho u D/\mu$) and Weber number ($We = \rho u^2 D/\sigma$), where ρ is the liquid density and D is the channel diameter. They stated their model was capable of predicting their experimental data within an accuracy of ±15% for $Ca < 0.25$.

For noncircular channels, Kolb and Cerro[16] studied the shape of the liquid film on the wall of a capillary of square cross-section by filling the capillary with a viscous fluid and then injecting air. They stated the shape of the liquid interface in the radial plane could be either noncircular or circular as shown in Figure 1, depending on the value of Ca. The noncircular interface was found to be is prominent at small Ca conditions. As Ca increases, the film thickness in the corners increases whilst the thickness on the sides remains almost

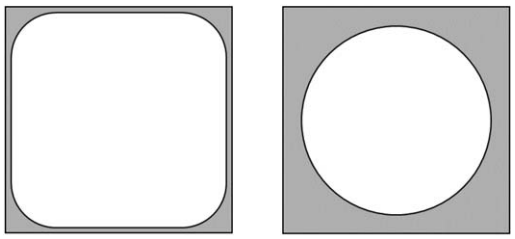

Figure 1. Sketch of (a) noncircular and (b) circular shape of fluids interfaces in square channel, proposed by Kolb and Cerro.[16]

unchanged. As *Ca* increases further, the interface becomes circular when *Ca* exceeds a critical value. Han and Shikazono[17] performed film thickness measurement of air bubbles in square microchannels of 0.3–1.0 mm hydraulic diameter, confirming the finding of Kolb and Cerro[16] regarding the evolution the shape of the interface. They developed an empirical correlation, dependent on *Ca* and *We*, for the prediction of film thickness on both the side and in the corners of the geometry achieving ±5% accuracy for $Ca < 0.4$.

Some correlations for film thickness that have been presented in the literature are summarized in Table 1. Most of these existing models calculate *Ca* on the basis of the bubble velocity,[9–11,13,15,17] while the correlation developed by Irandoust and Andersson[12] used the combined superficial velocity of both phases.

Despite a wealth of research for circular and square geometries, there is a dearth of studies for other geometrical shapes. Technologies used for fabrication of microchannels, such as etching or soft lithography, can lead to other more complex cross-sectional shapes, either by design or because of limitations of the method. The successful operation of microfluidic devices for multiphase reactions or for the creation of novel drop structures requires understanding of the ability to change over from one (miscible or immiscible) fluid to another, either for cleaning or to bring the different phases into contact. As shown above, correlations developed for circular channels are not always applicable for channels of other cross-sectional shapes, or for ranges of *Ca* which are lower than typically applied for cleaning of channels. This study addresses this gap in the literature by examination of displacement of one immiscible fluid by another less viscous fluid in channels with a complex near-semicircular shape (as found in a commercially available microfluidic chip), as well as circular and square channels. The thickness of the residual liquid film is examined for values of $0.02 < Ca < 80$. The effects of viscosity ratio, the viscosity of the liquid being displaced, the size of channel and the addition of a surfactant (SDS) into the displacing liquid have been investigated.

Materials and Methods

Microchannels

Three cross-sectional geometries were used: near-semicircular, circular, and square. The near-semicircular was selected from a commercially available microfluidic chip (Dolomite® Microfluidics, see the single straight channel in Figure 2a). Both circular and square channels were made in-house (Figure 2b). Table 2 gives the dimensions of the microchannels used.

The in-house geometries were made from an outer square glass capillary (borosilicate glass, inner size 1 × 1 mm, 55 mm in length, CM Scientific) and an inner capillary which was either round or square (various diameters, approx. 70 mm in length, CM Scientific). The inner capillary, which formed the main channel, was inserted into the outer square capillary and glued in place on a glass slide, ensuring the inner capillary remained aligned along the axis of the outer capillary. Water was injected into the gap between two capillaries before they were fixed in place, to minimize image distortion. PTFE tubing was used to provide connections at both the inlet and outlet of the channels. The fabrication steps are shown in brief in Figure 2c and the schematics of the cross-sections of these in-house channels are shown in Figure 2d.

Materials

Two immiscible fluids are used in each experiment: the fluid that is used to prefill the channel (initially stationary) is defined as the *displaced fluid* and the injected fluid is defined as the *displacing fluid*. Various fluid pairs were chosen with different kinematic viscosity ratios ($\eta = v_1/v_2$), shown in Table 3. All silicone oils were supplied by Sigma-Aldrich and 99.5% glycerol was supplied by ReAgent. To study the effect of the addition of a surfactant, Sodium Dodecyl Sulfate (SDS, ReagentPlus®, Sigma-Aldrich) was added to the *displacing fluid* at a concentration of 16.4 mol m^{-3}, which is twice of the critical micelle concentration (CMC). This concentration was chosen to ensure that the interfacial tension was no longer influenced by the concentration as it is well above the CMC. In addition, an estimation of surfactant balance using the maximum adsorption value shows that the percentage of surfactant at the interface does not exceed 2%, meaning the surfactant concentration in fluid the bulk of the *displacing fluid* is very close to its initial concentration of 2 × CMC.

Equilibrium interfacial tension values, σ_s, were measured with a Krüss K100 tensiometer, using the Wilhelmy plate

Table 1. Relevant Literature Correlations for Film Thickness

Reference		Correlation	Range of Applicability
Fairbrother and Stubbs[9]		$\frac{a}{D} = 0.25Ca^{0.5}$	$Ca \leq 0.09$ (Stated by Bretherton[11])
Bretherton[11]		$\frac{a}{D} = 0.67Ca^{2/3}$	$Ca \leq 0.01$
Data from Taylor[10]		$\frac{a}{D} = \frac{0.67Ca^{2/3}}{1+3.35Ca^{2/3}}$	$Ca \leq 1.4$
Correlation fitted by Aussillous and Quere[14]			
Irandoust and Andersson[12]		$\frac{a}{D} = 0.18\left(1-e^{(-3.08Ca^{0.54})}\right)$	$Ca < 2.0$
Han and Shikazono[15,17]	Circular channel	$\frac{a}{D} = \frac{0.67Ca^{2/3}}{1+3.13Ca^{2/3}+0.504Ca^{0.672}\mathrm{Re}^{0.589}-0.0352We^{0.629}}$	$Ca < 0.25$ and $\mathrm{Re} < 2000$
	Square channel	$\frac{a}{D} = \frac{1.215Ca^{2/3}}{1+7.28Ca^{2/3}-0.255We^{0.215}} - 0.0855$	$Ca < 0.4$

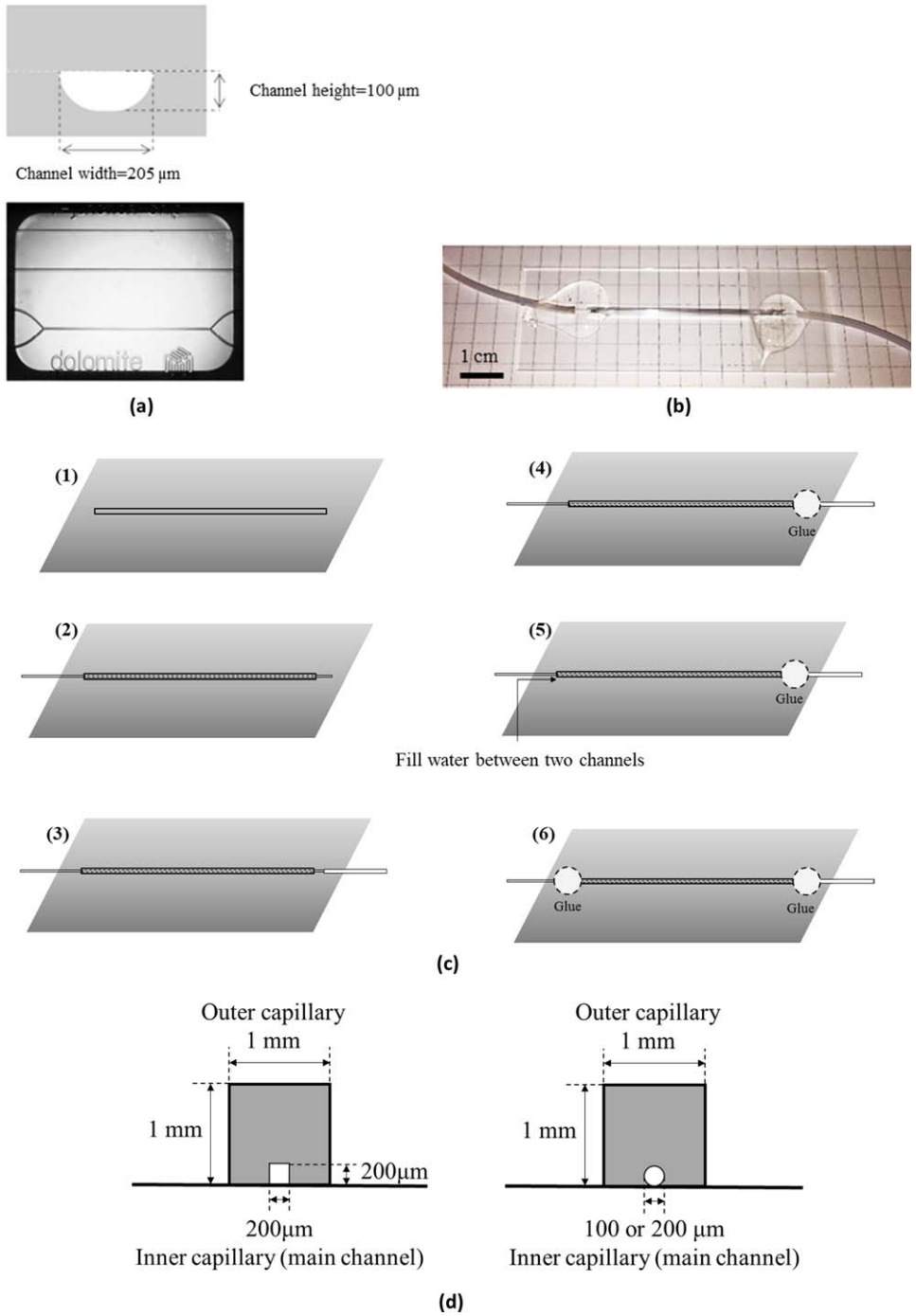

Figure 2. (a) Near-semicircular channel (microfluidic chip from Dolomite); (b) in-house device; (c) fabrication steps used in manufacture of the in-house device; (d) Schematics of the cross-sections of the in-house devices.

[Color figure can be viewed at wileyonlinelibrary.com]

method. For the purpose of flow visualization, the *displacing fluid* was dyed with black Nigrosin dye (water soluble, Sigma-Aldrich). It was found that the interfacial tension values between immiscible fluids were slightly affected by the presence of the dye and its concentration. Table 4 lists the equilibrium interfacial tension values for the *displacing fluid* dyed with Nigrosin at a concentration of 10 g L^{-1}.

Dynamic surface tension (the *displacing fluid*/air interface) values for the surfactant-laden *displacing fluid* were measured using a SINTERFACE BPA-1S maximum bubble pressure tensiometer and are shown in Figure 3. Dynamic surface tension effects are more observable at short timescales, a decrease from 50.5 to 38 mN m^{-1} is observed between surface ages from 0.7 ms to 0.1 s.

The dynamic surface tension values are used to estimate the dynamic interfacial tension between the *displaced fluid* and the *displacing fluid* with SDS added, following the strategy below, which was proposed recently[18]

$$\frac{\gamma_0-\gamma_s}{\sigma_0-\sigma_s}=\frac{\gamma_0-\gamma_{st}}{\sigma_0-\sigma_{st}} \tag{1}$$

Where γ_0 is the measured surface tension of surfactant-free dyed water, γ_s is the equilibrium surface tension of surfactant-laden dyed water, σ_0 is the interfacial tension between the

Table 2. Dimensions of Microchannels used in this Work

	Near-Semicircular	Circular		Square
Size	205 μm width, 100 μm height	200 μm diameter	100 μm diameter	200 × 200 μm
Hydraulic diameter (μm)	124.6	200	100	200
Source	Dolomite® Microfluidics	Made in the lab		

Table 3. Fluid Pairs Used in this Study

The Displaced Fluid	The Displacing Fluid	η
Silicone oil (10^{-4} m^2 s^{-1})	Water	100
	Glycerol solution (2×10^{-6} m^2 s^{-1}, 26.0% wt.)	50
	Glycerol solution (5×10^{-6} m^2 s^{-1}, 48.5% wt.)	20
	Water + SDS	100
	Glycerol solution + SDS (2×10^{-6} m^2 s^{-1})	50
	Glycerol solution + SDS (5×10^{-6} m^2 s^{-1})	20
Silicone oil (5×10^{-5} m^2 s^{-1})	Water	50
	Glycerol solution (2.5×10^{-6} m^2 s^{-1}, 32.6% wt.)	20
Silicone oil (2×10^{-5} m^2 s^{-1})	Water	20

displaced fluid and surfactant-free dyed water, σ_s is the equilibrium interfacial tension between the *displaced fluid* and surfactant-laden dyed water, γ_{st} is the dynamic surface tension of surfactant-laden dyed water at specific surface age t, σ_{st} is the estimated dynamic interfacial tension between the *displaced fluid* and surfactant-laden dyed water at surface age t.

Experiment procedure

Figure 4 shows the experimental setup used in this study. The experiment is performed in the following steps: (1) prefill the channel with the *displaced fluid* through the inlet; (2) when the channel is fully filled, the displacing fluid needle is connected to the inlet tubing when a fluid drop starts to appear at the needle tip, ensuring no air goes into the tubing; (3) the *displacing fluid* is injected at desired flow rate using a syringe pump (Harvard PHD 2000). After each experiment the microchannel is flushed with ~50 mL of acetone and then air is injected into the channel with high flowrate, for ~5 min, to ensure no residual fluids remain in the channel.

Table 4. Equilibrium Interfacial Tension Values

The Displaced Fluid	The Displacing Fluid		Equilibrium Interfacial Tension, σ_s, (mN m^{-1})
Silicone oil	Water	No dye	39.7
		Dyed	27.5
	Glycerol water solution	No dye	34.9
		Dyed	25.2
	Water + SDS	No dye	12.9
		Dyed	10.1
	Glycerol water solution + SDS	No dye	11.7
		Dyed	9.9

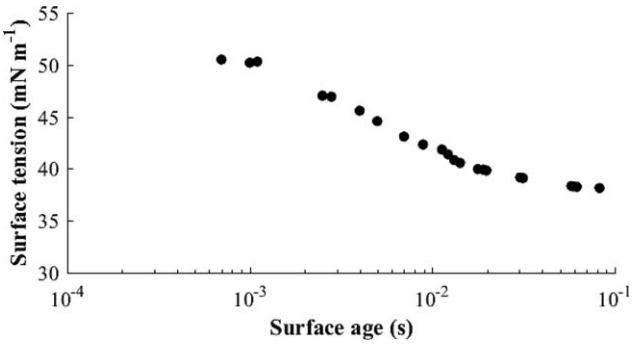

Figure 3. Dynamic surface tension of SDS in water solution (concentration two times CMC, dyed with 10 g L^{-1} Nigrosin).

The microchannels were placed on a microscope stage (Nikon TE2000-s inverted microscope, 4× lens). White light was used as the light source illuminating the channel from above and images were recorded through objective lens facing up toward the channel. The displacement process was recorded at the desired channel position using a high-speed camera (Photron FASTCAM SA3) attached to the microscope. The imaging position was fixed at ¾ of the total channel length from the channel inlet. Frame rates used were 4000–500 f.p.s. with shutter speeds set at 1–2 × 10^{-4} s.

Image analysis

The thickness of liquid film left on the channel wall following the passage of the tip of the *displacing fluid* was measured using the freeware ImageJ. The film thickness results were averaged from at least three repeats of each experiment. From the combination of the typical settings of the camera and the microscope lens used in this study, the pixel resolution in the recorded image is 2.17 μm. For some experimental images with low contrast, the background was subtracted from recorded image and binarized using Matlab, see Figure 5. It is noted that the film thickness does not stay unchanged during the whole displacement process. In this study, film thickness measurement is taken at the position of 2–2.5 times the width

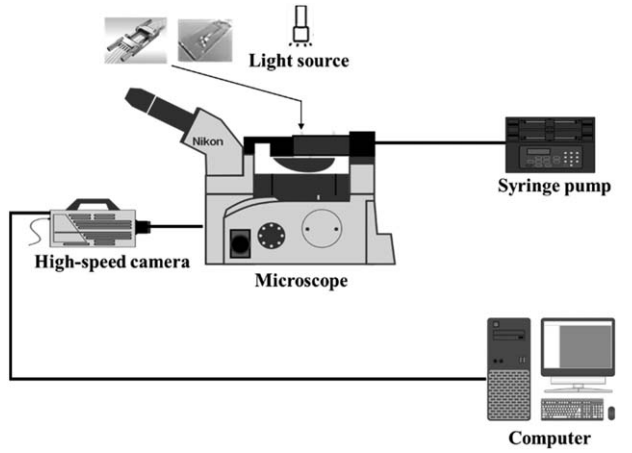

Figure 4. Experimental setup.

of the channel after the advancing of the *displacing fluid* tip, which is in some literature called initial film thickness.[19]

Theory

It has been widely accepted that the liquid film left on wall is not affected greatly by viscosity ratio especially for larger viscosity ratio (>10) cases,[20] thus capillary number based on the viscosity of the *displaced fluid* is used

$$Ca = \frac{\mu_1 u_2}{\sigma} \tag{2}$$

where μ_1 is the dynamic viscosity of the *displaced fluid*, u_2 is the mean velocity of the *displacing fluid,* and σ is the interfacial tension between the *displaced fluid* and *displacing fluid*. The superficial velocity of the *displacing fluid* is

$$u_2 = \frac{Q_2}{A_c} \tag{3}$$

where Q_2 is the injection flowrate of the *displacing fluid* and A_c is the cross-section area of channel. However, it is necessary to calculate the true velocity of the *displacing fluid*, u_2', to enable comparison with correlations. Thus, the superficial velocity needs to be corrected by determination of the true cross-sectional area occupied by the *displacing fluid*. The real *displacing fluid* velocity is thus calculated by dividing the injection flow rate of the *displacing fluid* by the cross-section area of the *displacing fluid* obtained from the thickness measurements. For the circular and square channels, it is assumed the cross-sectional area of the *displacing fluid* is always circular or very close to circular, explained in later section.

For near-semicircular channel, the strategy of estimating the shape of the cross-section of the *displacing fluid* is as follows: when film thickness is small, the shape is assumed to be an ellipse with the minor axis being the height of channel, H, and the major axis being the width of the *displacing fluid* (Figure 6a); when film thickness is larger than a critical value, a_{cr}, the shape of is assumed to be circular (Figure 6b). This critical thickness value $a_{cr} = (W - H)/2 = 52.5\ \mu$m.

The real velocity of the *displacing fluid* is calculated from

$$u_2' = \begin{cases} \pi\left(\frac{H}{2}\right)\left(\frac{W-2a}{2}\right) & \text{(Near-semicircular channel, } a < 52.5\ \mu\text{m)} \\ \frac{Q_2}{\pi\left(\frac{W-2a}{2}\right)^2} & \text{(Near-semicircular channel, } a \geq 52.5\ \mu\text{m)} \\ \frac{Q_2}{\pi\left(\frac{D-2a}{2}\right)^2} & \text{(Circular and square channel)} \end{cases} \tag{4}$$

Where D is the hydraulic diameter of the circular or square channel. The capillary number based on the real velocity of the *displacing fluid*, Ca′ is thus

$$Ca' = \frac{\mu_1 u_2'}{\sigma} = \begin{cases} \frac{\mu_1 Q_2}{\pi\sigma\left(\frac{H}{2}\right)\left(\frac{W-2a}{2}\right)} & \text{(Near-semicircular channel, } a < 52.5\ \mu\text{m)} \\ \frac{\mu_1 Q_2}{\pi\sigma\left(\frac{W-2a}{2}\right)^2} & \text{(Near-semicircular channel, } a \geq 52.5\ \mu\text{m)} \\ \frac{\mu_1 Q_2}{\pi\sigma\left(\frac{D-2a}{2}\right)^2} & \text{(Circular and square channel)} \end{cases} \tag{5}$$

For the cases with surfactant added into the *displacing fluid*, the interfacial tension values in the equation above depend on the surface age, which in this study the surface age is estimated as time necessary for the *displacing fluid* to travel from the inlet to the measurement point. This value ranges from $\sim 6 \times 10^{-3}$ s to ~ 2 s while the equilibrium interfacial tension is reached at a surface age of $\sim 7 \times 10^{-2}$ s. Therefore, either the estimated dynamic or equilibrium interfacial tension values are used in these calculations depending whether the surface age is below or above the value of 7×10^{-2} s, respectively.

Due to the limitation of experimental set-up, the recorded experimental images are a projected view of the flows, therefore only the widest part of flows can be directly seen from images. The film thickness directly measured from these images is referred to as the *apparent film thickness*, a in this study. However, for square and especially for the near-semicircular channel, the apparent film thickness found from the distance of the widest part of the *displacing fluid* to the channel wall obviously does not represent the film thickness at all azimuthal positions in the channel. Therefore, a mean film thickness is proposed for noncircular channels

$$a_{mean} = \frac{A_c - A_2}{\frac{1}{2}(P_c + P_2)} \tag{6}$$

Where A_C and P_C are the area and perimeter of the channel cross-section, and A_2 and P_2 are the area and perimeter of the cross-section of the *displacing fluid*. Using the assumption

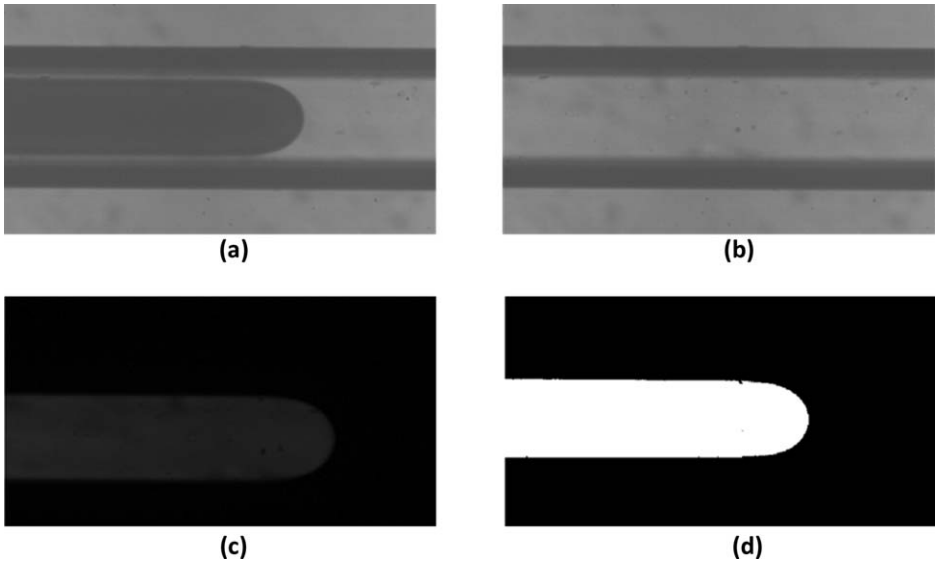

Figure 5. Image analysis of low contrast images (a): original target image; (b) background image; (c) subtraction of background image from target image; (d) binarized image.

made for the cross-sectional shape of the *displacing fluid* described above, for the near-semicircular channel the mean film thickness is calculated by dividing the cross-section area of the *displaced fluid* left on wall by the average length of the perimeters of the contour of the *displacing fluid* and the perimeter of the channel cross-section

$$a_{\text{mean}}=\begin{cases}\dfrac{A_C-\pi\left(\frac{H}{2}\right)\left(\frac{W}{2}-A\right)}{\frac{1}{2}\left\{p_c+\left(\pi\left(3\left(\left(\frac{W}{2}-A\right)+\frac{H}{2}\right)-\sqrt{\left(3\left(\frac{W}{2}-A\right)+\frac{H}{2}\right)\left(\left(\frac{W}{2}-A\right)+\frac{3H}{2}\right)}\right)\right)\right\}} & (\text{a}<52.5\,\mu\text{m})\\ \dfrac{A_C-\pi\left(\frac{W}{2}-A\right)^2}{\frac{1}{2}\left(p_c+\pi(W-2a)\right)} & (\text{a}\geq 52.5\,\mu\text{m})\end{cases} \tag{7}$$

Similarly, for square channel the mean film thickness is calculated from

$$a_{\text{mean}}=\frac{A_c-1/4\pi(D-2a)^2}{1/2(P_c+\pi(D-2a))} \tag{8}$$

Results and Discussion

In this study, the film thicknesses presented are normalized by the channel hydraulic diameter and the modified capillary number, calculated from Eq. 5, is chosen to represent more accurate estimation of the viscous effects. The deviation of the real *displacing fluid* velocity, u_2', from the *displacing fluid* superficial velocity, u_2, is obviously dependent on the film thickness as shown in Figure 7 for three channel geometries for surfactant-free fluid pairs. The ratio u_2'/u_2 increases as film thickness increases up to a maximum value of ~2.6 over the studied range.

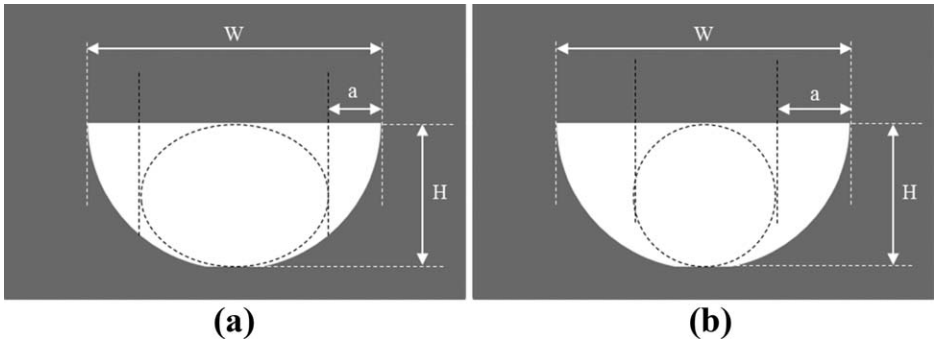

Figure 6. Proposed cross-sectional interface shapes in the near-semicircular channel: (a) ellipse shape; (b) circular shape.

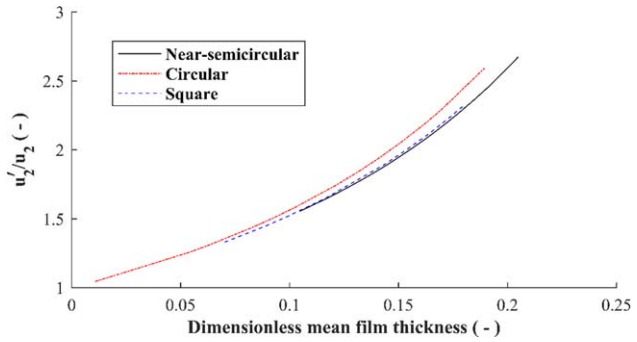

Figure 7. Ratio of u_2' to u_2 plotted against dimensionless mean film thickness for near-semicircular, circular and square channel using surfactant-free displacing fluid.

[Color figure can be viewed at wileyonlinelibrary.com]

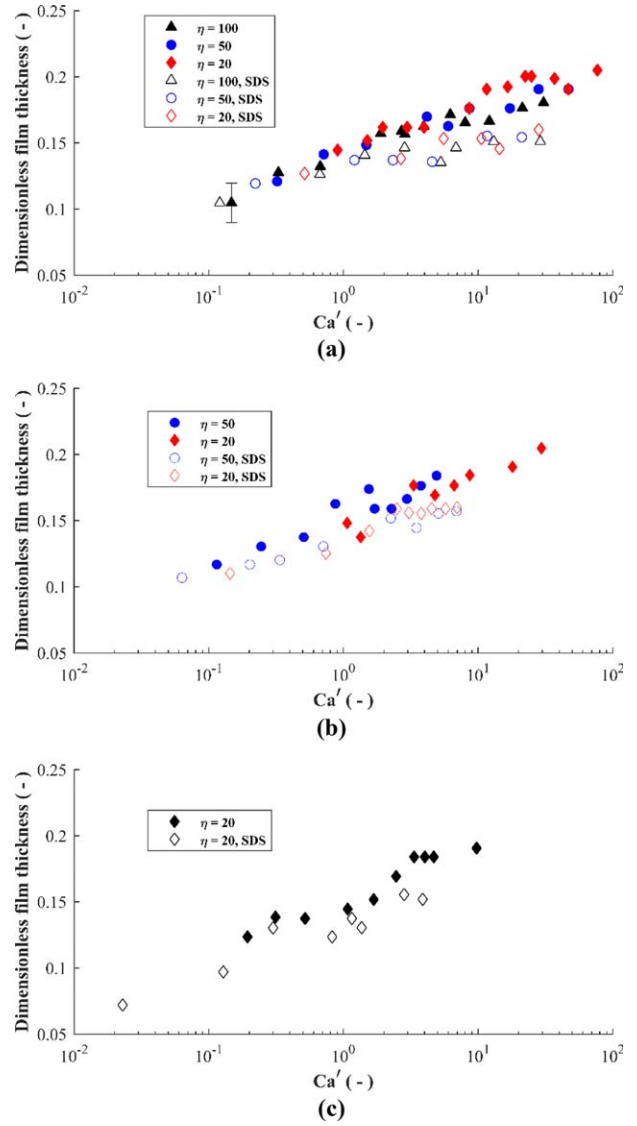

Figure 8. Dimensionless mean film thickness in near-semicircular channel for: (a) the *displaced fluid*- = 1 × 10^{-4} m^2 s^{-1} silicone oil, (b) the *displaced fluid* = 5 × 10^{-5} m^2 s^{-1} silicone oil, (c) the *displaced fluid* = 2 × 10^{-5} m^2 s^{-1} silicone oil.

[Color figure can be viewed at wileyonlinelibrary.com]

Effects of viscosity ratio (at constant viscosity of)

The effect of viscosity ratio between the two fluids is first examined using the near-semicircular channel. Plots of the dimensionless mean film thickness versus Ca′ for the cases using 1 × 10^{-4}, 5 × 10^{-5}, and 2 × 10^{-5} m^2 s^{-1} silicone oil as the *displaced fluid* are shown in Figure 8. The error bar in the figure represents the typical errors for these data points. Results using surfactant-free and surfactant-laden (SDS) fluids are both shown. As described above, dynamic interfacial tension values at corresponding timescales estimated from Eq. 1 were used to calculate Ca′ for the latter. Figure 8 shows that the dimensionless film thickness correlates well with Ca′; the data are weakly dependent on viscosity ratio. This could be due to operational and measurement error from the minimum resolution (2.16 μm) in this study. Thus, experimental data are plotted as a function of the *displaced fluid* for all viscosities of the *displacing fluid* used.

Validation of the mean film thickness approach

The values of dimensionless film thickness for the near semicircular channel are compared with the literature correlations to validate the above assumptions made for the shape of the interface between the two fluids. The results based on dimensionless apparent film thickness (empty symbols) and mean film thickness (filled symbols) are plotted in Figure 9 as a function of Ca′ alongside relevant literature correlations (Table 1). As the effect of viscosity ratio between the two fluids is insignificant, the results using 1 × 10^{-4} m^2 s^{-1} silicone oil as the *displaced fluid*, which contain three viscosity ratios, are grouped into a single data set. The same operation has been performed for the 5 × 10^{-1} m^2 s^{-1} silicone oil as the *displaced fluid*, which contains two viscosity ratios. The distance from the inlet to the position where film thickness is measured in the present study is around 17 mm, which is more than 100 times the hydraulic diameter of the near-semicircular channel. This means these literature models, most of which are developed from the measurement or analysis of the film thickness of long bubbles, can be used for comparison. Note the model developed by Irandoust and Andersson[12] used total average

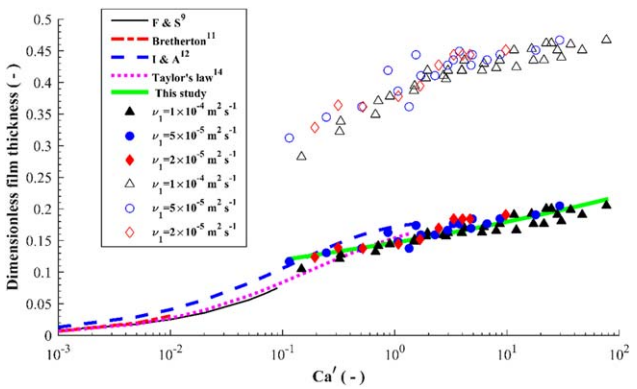

Figure 9. Dimensionless apparent and mean film thickness in near-semicircular channel, compared with available models from the researches of Fairbrother and Stubbs,[9] Bretherton,[11] Irandoust and Andersson,[12] and Taylor's law.[14] Filled markers represent results for mean film thickness and empty marks represent apparent film thickness.

[Color figure can be viewed at wileyonlinelibrary.com]

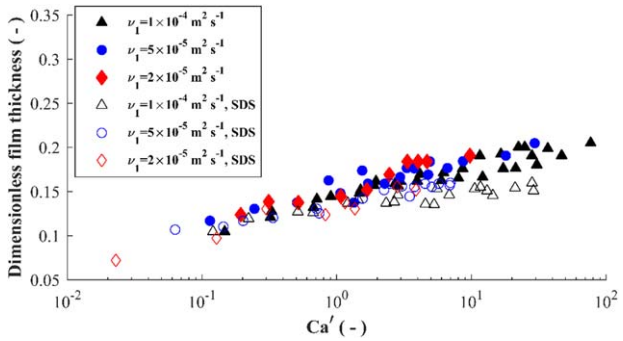

Figure 10. Comparison of film thickness using different viscosities of the *displaced fluid* in near-semicircular channel for SDS-free and SDS-laden cases.

[Color figure can be viewed at wileyonlinelibrary.com]

velocity, whereas all other models presented in Table 1 use bubble velocity to define the capillary number. This explains why the results of Irandoust and Andersson[12] are shifted to the left on Figure 9 because using bubble velocity results in an increase in the capillary number. Also they studied uprising bubbles in vertical channels where buoyancy can influence the results.

Figure 9 shows the apparent film thickness deviates considerably from literature predictions by approximately a factor of three, the apparent film thickness is not representative. Results obtained using the mean film thickness show good agreement. Using the Taylor's law equation developed by Aussillous and Quere,[14] the average variation between predicted dimensionless film thickness and the experimental data is 7%. Therefore it is proposed that the assumption of either elliptical or circular cross-section shape of the *displacing fluid* interface and the mean film thickness is an acceptable approach to estimate the overall film thickness for the near-semicircular channel in this study.

A film thickness correlation was developed using the experimental data of all fluid pairs without SDS added in the near-semicircular channel

$$\frac{a_{\text{mean}}}{D} = 0.147 Ca'^{0.0883} \tag{9}$$

This correlation describes the experimental data reasonable well ($R^2 = 0.843$) for $0.15 < Ca' < 80$, $1 < v_l < 100$, $20 < \eta < 100$. This correlation is added into Figure 9 for comparison. The proposed correlation generally follows the trend of the existing models extending them to larger values of capillary number at which the film thickness increases more slowly. This behavior is also observed in the model of Irandoust and Andersson.[12]

Effects of the displacing fluid viscosity

The effect of the viscosity of the *displaced fluid* was examined using three silicon oils with kinematic viscosities of: 1×10^{-4}, 5×10^{-5} and 2×10^{-5} m^2 s^{-1} respectively. As above, the results obtained using the same *displaced fluid* but with different viscosity ratios are grouped together, as the data are weakly dependent on viscosity ratio. Figure 10 shows results for both surfactant-free and surfactant-laden (SDS) *displacing fluid*. The figure shows that the data are also weakly dependent on the viscosity of the *displaced fluid* over the chosen range, especially at low capillary numbers. When $Ca' \gg 1$, the film thickness for 5×10^{-5} and 2×10^{-5} m^2 s^{-1} silicone oil appears to be slightly larger than that of 1×10^{-4} m^2 s^{-1} silicone oil and this is observed in both surfactant-free and surfactant-laden cases. These results confirm some literature findings: Han and Shikazono[15] studied the displacement of three liquids by air: water, ethanol and FC-40 liquid, which are respectively ~3.7 times and 3 times more viscous than water and ethanol in terms of dynamic viscosity and around 2 times and 1.3 times more viscous than water and ethanol in terms of kinematic viscosity. It was found for $0 < Ca < 0.08$ for all three fluids or for $0 < Ca < 0.15$ for ethanol and FC-40, the more viscous fluid resulted in smaller film thickness. This effect was found to increase with increasing capillary number.

Effect of surfactant SDS

As the film thickness increases as Ca increases, by definition, an increase of viscosity and/or velocity or a decrease of interfacial tension should lead to an increase of the film thickness. For surfactant-laden *displacing fluid*, the most obvious difference that surfactant molecules bring is the change of interfacial tension. It can be seen from Figure 10 that even after taking the dynamic interfacial tension effects into consideration (via calculation of Ca′) there is an additional physical effect leading to a thinner liquid film than for the surfactant free cases at the same capillary number, especially at larger capillary number conditions. Although there are inaccuracies in the estimation of dynamic interfacial tension from Eq. 1, explanation may be that other mechanisms come into play (Figure 11).

It is well known that recirculatory flows can develop inside the penetrating fluid tip and also in the *displaced fluid*, as postulated by Taylor.[11] When flow rate of the *displacing fluid* is small, this effect is small and the new interface between the two fluids generated at the channel inlet remains relatively undisturbed. In this case the dynamic interfacial tension, or equilibrium interfacial tension for some small Ca′ cases, is sufficient to describe the effect of surfactant migration to the new interface, based on the timescale of the fluid flow that is, $t = L/u_2'$, and the behavior is similar to that of pure liquids at low

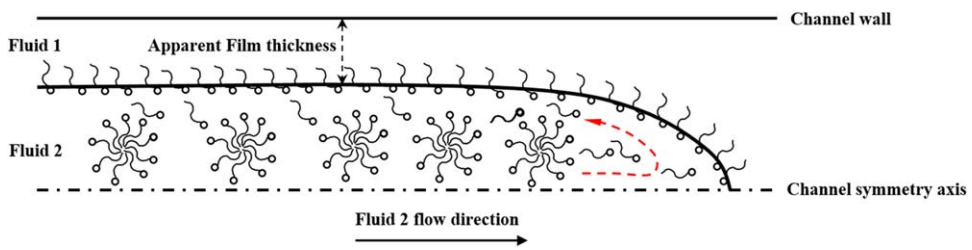

Figure 11. Schematic illustration of the problem of surfactant-laden the *displacing fluid* (size of molecules is not to scale).

[Color figure can be viewed at wileyonlinelibrary.com]

values of Ca′. However as the *displacing fluid* flow rate increases, the recirculation effect becomes larger as illustrated by the arrow in Figure 11. In this case the surfactant at the interface at the leading edge of displacement the will be convected toward the back leading to depletion at the tip if the bulk diffusion of surfactant from the bulk to the interface is not sufficient to replenish it. This local effect could lead to higher surface tension close to the tip and Marangoni stresses, resulting in a thinner liquid film on the wall. This thinning effect is contrary to findings found in the numerical simulations by Ratulowski and Chang[21] and Olgac and Muradoglu[22] for gas displacing a liquid laden with surfactant; they observed an increase in the film thickness. Reasons for this discrepancy most probably are due to difference in conditions used in mentioned simulations and in the present work. First, both numerical studies considered an air bubble moving in the surfactant-laden liquid. In this case the bubble front surface is always in contact with surfactant solution of initial concentration, whereas surfactant depletion occurs along the bubble due to surfactant adsorption from the thin liquid film to the liquid/air interface. In the present study surfactant is situated in the displacing liquid. Therefore, depletion can occur at the leading edge of displacement due to Taylor convection. Both numerical studies are related to low capillary numbers, $Ca < 10^{-1}$, whereas surfactant-related changes in the film thickness were observed in the present study at $Ca > 1$. Ratulowski and Chang[21] assumed the equilibrium between the interfacial and bulk surfactant in the uniform film region, but because of high flow rates, equilibration between surfactant in the bulk and at the interface was not achieved in the present study at flow rates where the film thinning was observed.

Olgac and Muradoglu[22] used the effective surface tension related to the average surfactant concentration on the liquid/air interface to calculate the capillary number. Due to the nonuniform surfactant distribution, the film thickness was larger when compared to the film formed by the pure liquid of the same surface tension in the central part of the bubble (quasi-uniform film), but was smaller than the pure liquid film in the transition zone near the front of the bubble. For the largest capillary number considered by Olgac and Muradoglu,[22] $Ca = 0.097$, the film thickness for the case of an insoluble surfactant was smaller than that formed by pure liquid with the same surface tension in the quasiuniform film part. Therefore, based on the results of Olgac and Muradoglu,[22] it can be assumed that by an increase of capillary number and the corresponding decrease of characteristic time of surfactant adsorption, a soluble surfactant can demonstrate similar behavior, that is, produce a smaller film thickness.

Note, the surfactant used in this study is characterized by very fast equilibration at concentrations above CMC when compared with other commonly used surfactants.[23] Therefore, a comprehensive study of other surfactants with different CMC values and in a range of concentrations is required to make more general conclusions on the effect of surfactant on the film thickness. It can be suggested from the discussion above that if an increase in the film thickness is due to depletion of surfactant from the leading edge of displacing liquid then using slower equilibrating surfactants, such as Triton X-100 or hexadecytrimethylammonium bromide (CTAB)[23] should result in further decrease of film thickness, whereas increase in concentration of SDS or other quickly equilibrated surfactant (e.g., dodecyltrimethylammonum bromide[18])will eventually increase the film thickness back to the value expected for the capillary number based on surface tension of surfactant solution.

Effect of channel size and geometry

The effect of channel shape was studied using two circular channels of 200 and 100 μm inner diameter and a 200 μm square channel. 1×10^{-4} m^2 s^{-1} silicone oil is used as the *displaced fluid* and viscosity ratios of 20, 50, and 100 were studied by varying the viscosity of the *displacing fluid*.

Dimensionless film thicknesses for both 200 and 100 μm circular channels are plotted against Ca′ in Figure 12. The apparent film thickness is used for circular channel, because in this case the mean film thickness is equal to the apparent thickness. The results show that the dimensionless film thickness is larger for the larger channel when $Ca' > 1$. A similar trend was observed by Aussillous and Quere,[14] who used channels with diameters from 0.4 to 1.4 mm for $Ca < 0.05$ and by Han and Shikazono[15] who used channels of 0.3–1.3 mm diameter for $Ca < 0.08$. However the results reported by Tsaoulidis and Angeli,[24] who studied the film thickness in 0.5–2 mm channels, suggest an insignificant effect of channel size on the film thickness up to values of $Ca < 0.2$.

For square channels, the existence of corners causes the film thickness to be non-uniform. Therefore, the approach of mean film thickness is also applicable here. Dimensionless apparent and mean film thicknesses are both plotted in Figure 13, as well as the model developed by Han and Shikazono[17] and Taylor's law.[14] Most of the correlations for liquid film thickness do not take channel size into account explicitly and only consider capillary number. However, Han and Shikazono[15,17] have developed empirical equations using both Weber number and Reynolds number in addition to capillary number. Figure 13 shows the film thickness values obtained from the Han and Shikazon[17] correlation for square channels recalculated on the basis of the mean film thickness (Eq. 8).

It has been shown in previous study[16] that the thickening of the film in a square channel starts in the corners whereas the film thickness at the sides remains unchanged. Beyond a critical capillary number and a critical film thickness at the corner, the contour of the *displacing fluid* becomes circular and both the liquid film thickness at the corner and at the sides increases with further increase in capillary number. The dashed line in Figure 14 is an illustration of the possible contour of the *displacing fluid* interface at smaller capillary numbers. However the experimental images taken show a clear sharp layer of the *displaced fluid* film, under all conditions. Thus, the contour of

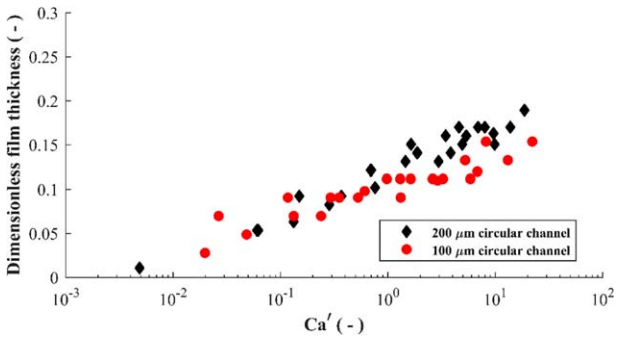

Figure 12. Dimensionless film thickness for 200 and 100 μm circular channels. The *displaced fluid*: 1×10^{-4} m^2 s^{-1} silicone oil.

[Color figure can be viewed at wileyonlinelibrary.com]

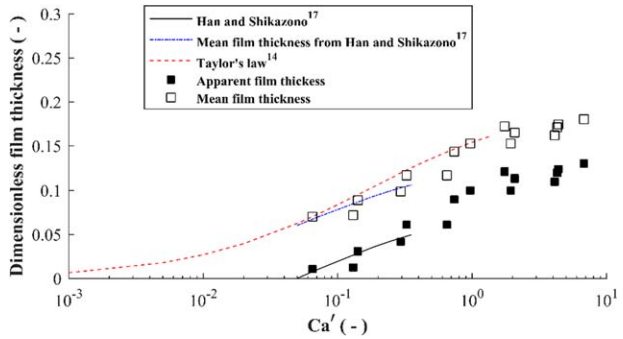

Figure 13. Results of apparent film thickness and mean film thickness for the square channel, the *displaced fluid* = 1 × 10^{-4} m^2 s^{-1} silicone oil, compared with Taylor's law[14] and Han and Shikazono.[17]

[Color figure can be viewed at wileyonlinelibrary.com]

the *displacing fluid* is always circular at the high capillary numbers in this study. This can be also assessed from the reported critical capillary number value, which in the experiments by Kolb and Cerro[16] is $Ca \sim 0.1$ and for Han and Shikazono[17] is $Ca \sim 0.02$.

The model of Han and Shikazono[17] used here is correlated with the thickness at the sides of the channel, which corresponds to the apparent film thickness. By comparing the experimental data with Han and Shikazono's empirical equations, good agreement is found for $Ca < 0.4$, which is the maximum value used in their study. The mean film thickness results are also in line with the recalculated mean thickness based on Han and Shikazono's[17] correlation. It can be seen that using the apparent film thickness at sides, experimental data does not fit to Taylor's law, which is developed using results in circular channel. However by calculating the mean film thickness using Eq. 8, the data fit is much improved. This demonstrates that the approach of mean film thickness is

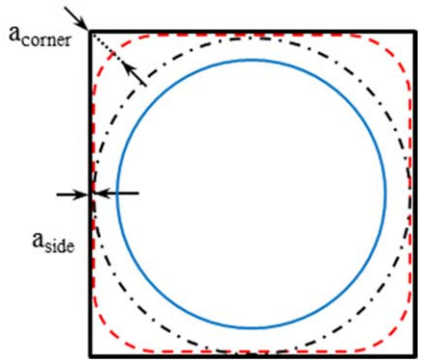

Figure 14. Illustration of the cross-section shape of the *displacing fluid* in square channel for smaller capillary number. Red dashed line: possible contour of the *displacing fluid* interface, blue solid line: assumed the *displacing fluid* interface in the mean film thickness approach, dot-dashed line: illustration of the inaccurate estimation of mean film thickness if the *displacing fluid* interface is noncircular.

[Color figure can be viewed at wileyonlinelibrary.com]

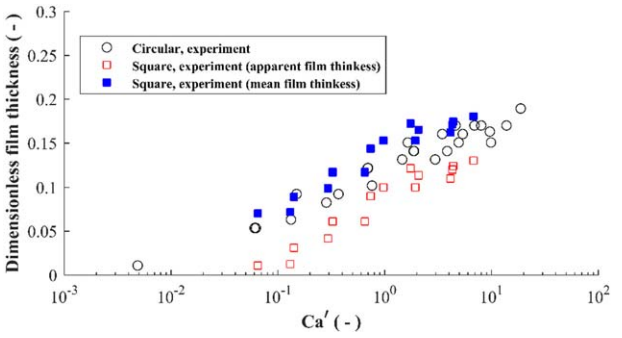

Figure 15. Dimensionless film thickness of circular and square channel with 200 um hydraulic diameter. The *displaced fluid* = 1 × 10^{-4} m^2 s^{-1} silicone oil.

[Color figure can be viewed at wileyonlinelibrary.com]

applicable not only to the near-semicircular channel but also to the square channel, which opens the possibility that this approach could be used for any noncircular channel if the contour of the interface in the cross-section can be either be known or assumed. In addition, this also agrees with the previous finding that under all conditions in this study, the *displacing fluid* presents a circular cross-section shape. This is because the equation for calculating the mean film thickness in square channel uses the assumption of circular interface shape. If the contour of the *displacing fluid* was not circular, using Eq. 8 will result in an overestimation of the mean film thickness as the thickness in the corner increases (shown as the dot dash circle in Figure 14).

Comparison of dimensionless film thickness for circular and square channels with the same hydraulic diameter (200 μm) is shown in Figure 15. For the square channel, both the apparent and mean film thickness are shown.

It can be seen that the film thickness results for circular channel are generally larger than the apparent film thickness measured in square channel. This agrees with the results of Han and Shikazono[15,17] who also studied both circular and square channels with the same size. The mean film thickness for square channel appears to be slightly larger than the film thickness for circular channel. This is because the method of calculating mean film thickness takes into consideration the corner area, where more liquid is likely to remain than in the circular channel.

Conclusions

An experimental study on the displacement of a more viscous fluid (the *displaced fluid*) by an immiscible less viscous fluid (the *displacing fluid*) has been performed using microchannels with near-semicircular, circular, and square cross-sections and hydraulic diameters from 100 to 200 μm. The film thickness was measured visually following the advancing fluid tip of the *displacing fluid*. The capillary number based on the viscosity of the *displaced fluid* and the real velocity of the *displacing fluid* is used as the main characterizing parameter. The values of capillary number used in this study, $0.02 < Ca < 80$, extended the previous reported range. Within the studied range of viscosities, the viscosity ratio between the two fluids and the viscosity of the *displaced fluid* have insignificant effect on the liquid film thickness. The film thicknesses obtained using 5 × 10^{-5} and 2 × 10^{-5} m^2 s^{-1} viscosity fluids as the *displaced fluid* are shown to be slightly

larger than when the *displaced fluid* has a viscosity of 1×10^{-4} m^2 s^{-1} and this effect increases with increasing capillary number. An empirical model describing the mean film thickness against modified capillary number, was proposed in this study, using the experimental data from near-semicircular channel and all fluid pairs without the addition of SDS. This correlation extends the existing models to higher capillary numbers where the increase of film thickness has a weaker dependence on capillary number.

A film thinning effect has been observed when a surfactant (SDS) is added into the *displacing fluid*, especially at large capillary numbers. This is believed to be the result of SDS redistribution caused by convective flows due to recirculation of fluid in the advancing tip.

For noncircular channels including the near-semicircular and square channel, the mean film thickness approach has been shown to be an effective way to estimate the overall film thickness. This is validated by comparing the mean film thickness for noncircular channels with literature models. It has also been shown that existing literature correlations can be extended to larger range of capillary number.

Acknowledgments

This research was funded by the EPSRC Programme Grant "MEMPHIS – Multiscale Examination of Multiphase Physics in Flows" (EP/K003976/1). Yu Lu was funded by a PhD studentship from the School of Chemical Engineering, University of Birmingham.

Notation

A_c = channel cross-section area
A_2 = cross-section area of the displacing fluid
a = apparent thickness measured from images
a_{corner} = film thickness at cross-section diagonal plane in square channel
a_{side} = film thickness at sides in square channel
a_{mean} = mean film thickness
Ca = capillary number without velocity modification
Ca' = velocity modified capillary number
D = hydraulic diameter of channel
H = height of channel
P_C = perimeter of the channel cross-section
P_2 = perimeter of the interface of the displacing fluid at cross-section
Q = flowrate 2 injection flowrate
Re = Reynolds number
u_2 = displacing fluid superficial velocity
u_2' = real displacing fluid mean velocity
W = width of channel
We = Weber number
γ_s = equilibrium surface tension
γ_{st} = surface tension with surfactant at surface age t
η = viscosity ratio (the displaced fluid/the displacing fluid)
γ_0 = surface tension without surfactant
μ_2 = dynamic viscosity of the displacing fluid
v_1 = kinematic viscosity of the displaced fluid
v_2 = kinematic viscosity of the displacing fluid
ρ_2 = density of the displacing fluid
σ = interfacial tension between two fluids
σ_s = equilibrium interfacial tension
σ_{st} = interfacial tension with surfactant at surface age, t
σ_0 = interfacial tension without surfactant

Literature Cited

1. Pamme N. Continuous flow separation in microfluidic devices. *Lab Chip*. 2007;7(12):1644–1659.
2. Yamada M, Nakashima M, Seki M. Pinched flow fractionation: continuous size separation of particles utilizing a laminar flow profile in a pinched microchannel. *Anal Chem*. 2004;76(18):5465–5471.
3. Huh D, Bahng JH, Ling Y, Wei HH, Kripfgans OD, Fowlkes JB, Grotberg JB, Takayama S. A gravity-driven microfluidic particle sorting device with hydrodynamic separation amplification. *Anal Chem*. 2007;79(4):1369–1376.
4. Okushima S, Nisisako T, Torii T, Higuchi T. Controlled production of monodisperse double emulsions by two-step droplet breakup in microfluidic devices. *Langmuir*. 2004;20(23):9905–9908.
5. Atencia J, Beebe DJ. Controlled microfluidic interface. *Nature*. 2005;437(7059):648–655.
6. Kobayashi J, Mori Y, Okamoto K, Akiyama R, Ueno M, Kitamori T, Kobayashi S. A microfluidic device for conducting gas-liquid-solid hydrogenation reactions. *Science*. 2004;304(5675):1305–1308.
7. Shestopalov I, Tice JD, Ismagilov RF. Multi-step synthesis of nanoparticles performed on millisecond time scale in a microfluidic droplet-based system. *Lab Chip*. 2004;4(4):316–321.
8. Sia SK, Whitesides GM. Microfluidic devices fabricated in poly(dimethylsiloxane) for biological studies. *Electrophoresis*. 2003;24(21):3563–3576.
9. Fairbrother F, Stubbs AE. Studies in electro-endosmosis. Part VI. The "Bubble-tube" method of measurement. *J Chem Soc*. 1935;527–529.
10. Taylor GI. Deposition of a viscous fluid on the wall of a tube. *J Fluid Mech*. 1961;10(02):161–165.
11. Bretherton FB. The motion of long bubbles in tubes. *J Fluid Mech*. 1961;10(02):166–188.
12. Irandoust S, Andersson B. Liquid film in Taylor flow through a capillary. *Ind Eng Chem Res*. 1989;28(11):1684–1688.
13. Ratulowski J, Chang HC. Transport of gas bubbles in capillaries. *Phys Fluids A*. 1989;1(10):1642–1655.
14. Aussillous P, Quéré D, Quick deposition of a fluid on the wall of a tube. *Phys Fluids*. 2000;12(10):2367–2371.
15. Han Y, Shikazono N. Measurement of the liquid film thickness in micro tube slug flow. *Int J Heat Fluid Flow*. 2009;30(5):842–853.
16. Kolb WB, Cerro RL. Coating the inside of a capillary of square cross section. *Chem Eng Sci*. 1991;46(9):2181–2195.
17. Han Y, Shikazono N. Measurement of liquid film thickness in micro square channel. *Int J Multiphase Flow*. 2009;35(10):896–903.
18. Kovalchuk NM, Roumpea E, Nowak E, Chinaud M, Angeli P, Simmons MJH. Effect of surfactant on emulsification in microchannels. *Chem Eng Sci*. 2018;176:139–185.
19. Li S, Sun C, Liu B, Feng X, Li F, Chen L, Chen G. Initial thickness measurement and insights into crystal growth of methane hydrate film. *AIChE J*. 2013;59(6):2145–2154.
20. Soares EJ, Carvalho MS, Souza Mendes PR. Immiscible liquid-liquid displacement in capillary tubes. *J Fluids Eng*. 2005;127(1):24–31.
21. Ratulowski J, Chang HC. Marangoni effects of trace impurities on the motion of long gas bubbles in capillaries. *J Fluid Mech*. 1990;210(1):303–328.
22. Olgac U, Muradoglu M. Effects of surfactant on liquid film thickness in the Bretherton problem. *Int J Multiphase Flow*. 2013;48:58–70.
23. Wang K, Zhang L, Zhang W, Luo G. Mass-transfer-controlled dynamic interfacial tension in microfluidic emulsification processes. *Langmuir*. 2016;32(13):3174–3185.
24. Tsaoulidis D, Angeli P. Effect of channel size on liquid-liquid plug flow in small channels. *AIChE J*. 2016;62(1):315–324.

Manuscript received Sep. 20, 2017, and revision received Mar. 14, 2018.